H-mode filament studies with reflectometry in ASDEX Upgrade

J Vicente[1], G D Conway[2], M E Manso[1], H W Müller[2], C Silva[1], F da Silva[1], L Guimarãis[1], A Silva[1] and the ASDEX Upgrade Team

[1] Instituto de Plasmas e Fusão Nuclear, Instituto Superior Técnico, Universidade de Lisboa, 1049-001 Lisboa, Portugal
[2] Max-Planck-Institut für Plasmaphysik, 85748 Garching, Germany

E-mail: jvicente@ipfn.ist.utl.pt

Abstract. Broadband swept (FM-CW) and fixed frequency reflectometry (FFR) were used for the first time to study plasma filamentary activity; experiments were performed in ELMy H-mode plasmas at the ASDEX Upgrade tokamak. Electron density profiles were first studied with FM-CW providing a first insight into filamentary activity and enabling to localize the density layers probed with FFR. A novel filament detection technique was developed using the values higher than a selected threshold on the FFR phase derivative signals as indicators of filaments. This technique was applied together with conditional averaging in measurements performed in the vicinity of the separatrix. Results are in good agreement with data from Langmuir probes and it was found that the majority of filaments propagate with dominant poloidal velocity in both inter-ELM periods ($V_\theta \approx 575$ m/s) and at the ELM onset ($V_\theta \approx 1180$ m/s). A time delay between the maximum filament activity at the outer mid-plane and the ELM peak at the inner divertor currents (≈ -461 ± 50 μs) agrees with expected time scales for the ELM lifetime. In inter-ELM periods we were able to estimate typical poloidal and toroidal sizes of filaments ($S_\theta \approx$ [5.75-11.50] cm and $S_\phi \approx$ [33-66] cm) and an MHD mode structure emerged from the measurements with poloidal and toroidal mode numbers (m ≈ [8-12] and n ≈ [2-3]) in the range of possible ballooning modes.

1. Introduction

Plasma filaments are coherent structures of high plasma density observed in the edge plasma of most magnetic confinement devices in both low (L-mode) and high confinement (H-mode) operation regimes (see [1-4] and references therein). Their nature is still not fully understood but increasing experimental work has characterized filaments and their dynamics. The plasma filaments have a 3-D spatial structure with pronounced toroidal elongation along the magnetic field lines. In medium sized tokamaks the toroidal extent of plasma filaments is of metres while the poloidal size is of few centimetres and typically larger than the radial size. Variations on the average values and probability distribution functions of the filament parameters are found depending on the specific plasma regime and time period in which filaments occur, e.g. L-modes, type-I, type-II or type-III ELMs, or inter-ELM periods (see previous references). While a peeling-ballooning instability (currently favoured to explain the ELM cycle) is expected to develop flute-like ripples (e.g. n ≈ 5-20 [5]) in the pedestal quantities which later grow in magnitude and result in a sudden burst of distinct plasma filaments at the type-I ELM crash period [6], the existence of filaments in other periods of the ELM cycle and

other plasma regimes suggests the possibility of different generation mechanisms. In fact, ELM filament measurements indicate a birth region close to the pedestal top or further inside [7] whereas for filaments occurring in Ohmic discharges the generation region has been identified with the separatrix and the location of maximum electron pressure gradient (this could even be slightly outwards of the separatrix) where maximum linear growth rates of plasma instabilities driven solely by pressure gradient would occur [8].
In any case, filaments can be expelled out (of the Last Closed Flux Surface - LCFS) developing a radial velocity component that dominates their motion and drives them across the Scrape-Off Layer (SOL). It has been suggested that the interchange instability driven by radial gradients in plasma pressure and magnetic field curvature is responsible for the required outward acceleration [9, 10]. When travelling in the SOL they can either end up fading into the divertor or depositing their remaining particle and energy content on the inner walls of the fusion devices, depending on the competition between the parallel and the radial transport channels [11].
Intermittent transport across the edge plasma has been well characterized over the years (see [12-14] and references therein), and although intermittency has been recognized as an effect of the activity of filamentary structures, important questions remain open, such as: (i) how and where are filamentary structures born and (ii) what is the impact of the filaments on the plasma facing components and how does it scale to future experiments such as ITER. While a reasonable amount of data has already been collected to answer the last question, for fundamental understanding of filaments is also required data from the edge plasma region inside the separatrix with high spatial and temporal resolutions, which most diagnostics of fusion devices cannot provide. A microwave reflectometer is one of the few diagnostics that is *a priori* a good candidate to fulfil this task because it can have high resolution in both time and space and is able to measure coherent density perturbations propagating in the background turbulent plasma over a broad radial region. Reflectometry is a well established technique in diagnosing fusion plasmas that is based on radar instruments designed to detect density perturbations and density profiles in turbulent plasmas [15, 16]. With this technique, microwaves are launched into the plasma and are reflected at some density layer n_{ec} where a frequency “cut off" occurs. This critical density layer is determined solely by the launched frequency, for waves travelling with ordinary polarization (O-mode). Using different frequencies (usually swept in time), reflectometry can measure the position of several electron density layers to obtain the plasma density profile. When operated in fixed frequency the reflectometry measurements are sensitive to plasma density fluctuations essentially occurring locally at the reflecting plasma density layer. Doppler reflectometry, based on oblique incidence of the microwave and measurement of a Bragg backscattered signal, was previously used to demonstrate the possibility to investigate plasma filaments with that technique [17].

2. Experimental conditions and reflectometry capabilities

2.1. Experimental set-up and techniques

ASDEX Upgrade (AUG) is a medium sized diverted tokamak ($R \approx 1.65$ m, $a \approx 0.5$ m) with a fully tungsten coated first wall and equipped with versatile auxiliary heating and current drive systems so that different plasma regimes can be obtained within the allowed operational space [18]. H-modes are routinely produced in the so-called lower-single null (LSN) configuration and type-I ELMs can be easily monitored through currents measured on tile shunt resistances placed in the lower divertor. To help in characterizing the plasma edge a reciprocating manipulator located above the mid-plane ($z = 0.31$ m) on the low field side (LFS) is often used to plunge Langmuir probes into the plasma SOL. This allows local measurements at different radial positions, namely of the ion saturation current, I_{sat}. This parameter provides a time signal proportional to the plasma density which has been extensively used to detect and characterize plasma filaments in the SOL [7].

Two O-mode reflectometry systems with frequency hopping capability and operating in the microwave bands Q (33-49.2 GHz) and V (49.4-72 GHz) respectively have been the main diagnostics used in this work [19]. Both systems use mono-static antennas located on the LFS at the same toroidal position. The Q-band antenna is slightly above the mid-plane and the V-band antenna is about 32 cm below in the poloidal direction (see figure 1). The systems are equipped with heterodyne receivers and in-phase/quadrature detection schemes thus allowing to produce phase $\varphi(t)$ and amplitude $A(t)$ signals of the reflected wave. Both signals are reconstructed by previous calibration of the offsets and imbalances [20]. Furthermore, the Wang/Seo algorithm [21] is employed to minimize errors in the phase reconstruction caused by possible phase jumps of $\pm\pi$, due to finite sampling rate. Under the 1D geometric approximation the phase shift $\Delta\varphi$ of the reflected wave is proportional to a radial displacement Δr of the reflecting density layer, $\Delta r=\Delta\varphi c/4\pi F_o$ where c is the velocity of light and F_o is the microwave probing frequency [22]. The data acquisition rate of the reflectometry hopping systems is 2 MHz giving a temporal resolution (0.5 μs) suitable to resolve fast events such as filaments. The plasma region that can be probed by each reflectometry system is determined by the operational frequency range of each channel since the critical density n_{ec} is proportional to $(F_o)^2$ for O-mode waves. The density range is for Q-band: 1.35 – 3.00 x10^{19}m^{-3} and for the V-band: 3.01 – 6.43 x10^{19}m^{-3}. Regarding the spot sizes of the beams, the half power beam width (w) of the V-band and Q-band systems at their focusing distances are approximately 7º and 9º, respectively, or $w_{10dB} \approx 2.5$ cm and 6 cm [23]. The measuring limits of the instrument are determined by the beam width and the probing wavelength. These will determine the critical dimensions of a density perturbation below which a strong attenuation of the reflectometry signals together with loss of phase response is expected. An estimate for these limits can be obtained from simulations using 2D models and sinusoidal density perturbations [24]. Considering that the typical spatial scale L_{fil} of a filament can be described as half-wavelength of a sinusoidal perturbation, we can extrapolate (from the 2D surface distortion models) and expect *blindness* of the reflectometers for $L_{fil} << w$ i.e. a few cm.

In this work, dedicated experiments of deuterium plasma discharges were performed with simultaneous measurements by Langmuir probes mounted on a midplane manipulator and fixed frequency reflectometry (FFR). Measurements were obtained in the ELMy H-mode period of the LSN discharge #26981 with a plasma current of I_p = 1.0 MA, toroidal magnetic field of B_t = -2.58T (ion drift direction towards lower X-point), safety factor at the flux surface enclosing 95% of the total poloidal flux q_{95} = 4.7, Ohmic power P_{Ohm} = 0.4 MW, electron cyclotron resonance heating P_{ECRH} = 0.5 MW, neutral beam injection P_{NBI} = 5.0 MW and line integrated core plasma density $\overline{n_e}$ = 8.1 x10^{19}m^{-3}. Both hopping reflectometry systems were operating at their lowest possible frequencies in order to probe the most further out density layers possible, coinciding in radial positions close to where the Langmuir probe measures.

The actual radial positions of the density layers being probed by FFR must be known from a density profile measurement. AUG is equipped with additional O-mode reflectometry systems comprising K, Ka, Q, V, and W microwave bands that operate in fast frequency sweeps (FM-CW) and allow reconstructing the electron density profile. At the present fastest repetition rate, a profile can be obtained every 35 μs [25, 26]. While the radial position of the density layers can be obtained directly by the FM-CW system in length units [m], it is also common at AUG to use a normalized poloidal flux radius (ρ_{pol}) to describe the edge plasma. This coordinate is scaled such that ρ_{pol} = 0 on the magnetic axis and ρ_{pol} = 1 at the separatrix.

2.2. The H-mode density profile and the microwave beam access

We focused our analysis in H-mode regimes with type-I ELMs for two main reasons: i) enhanced filamentary activity during the so called ELM crash period ii) improved quality of the reflected signals due to the steep H-mode pedestal gradients and the reduced density fluctuations [27].

The ELMy H-mode generally features a cyclic repetition of periods with a sudden relaxation leading to the abrupt collapse of the edge pedestal (ELM crash) followed by a recovery phase. In figure 2 is

shown a set of averaged density profiles in the different phases of a typical ELM cycle measured by the FM-CW reflectometry system. The range of densities that can be probed by the Q and V channels of the FFR is indicated in the figure, as well as the minimum probed density layers $n_{e1} \approx 1.35 \times 10^{19} m^{-3}$ (Q channel operating at 33 GHz) and $n_{e2} \approx 3.01 \times 10^{19} m^{-3}$ (V channel at 49.4 GHz). As can be seen from figure 2, in inter-ELM periods the probed plasma regions lie in the steep pedestal area. Therefore, the minimum density layers n_{e1} and n_{e2} probed by each channel are very close in the radial coordinate. These density layers are located in the vicinity of the separatrix ($R_{sep} = 2.148 \pm 0.005\ m$) and so, probing layers in the far SOL should not be expected. However, it may be possible to detect filamentary structures outside and far away from the separatrix providing they are have sufficient density ($n_e > n_{e1}$) to reflect the probing microwaves.

2.3. Plasma filaments at AUG

Many studies on plasma filaments have been conducted in AUG using systems such as electrostatic probes, electron cyclotron emission, and gas-puff imaging [4, 7, 8, 15, 27-32]. The typical widths of filaments found are: toroidal width $S_\phi \approx$ [50-80] cm; poloidal width $S_\theta \approx$ [6-10] cm and radial width $S_r \approx$ [0.3-3] cm. Filaments with densities of more than twice the background density have been reported in the AUG SOL and far-SOL with peak density values up to $4 \times 10^{19} m^{-3}$ in the case of ELM filaments [7]. The propagation velocity of filaments both poloidal and radial are of few km/s, typically ≈ 1-2 km/s. Thus, many filaments should in principle be resolved in time and space by the reflectometry systems at AUG.

3. Reflectometry measurements

3.1. FM-CW reflectometry - density profile dynamics

The dynamics of the density profile during the ELM cycle were studied taking advantage of the fast repetition rate of the FM-CW system (a profile is measured every 35 μs). In figure 3 the time evolution of the position of some selected density layers is shown. The density profile crash at each ELM is clearly observed as well as the collapse and recovery phases along the pedestal region. We observe longer relaxation times for density layers close to the pedestal top than for those at the pedestal bottom that seem to react more promptly both in the collapse and the recovery phases. Further information is obtained by analyzing the statistical moments of the data, such as the standard deviation and the skewness. We observe reduced fluctuation levels (i.e. reduced standard deviations) for densities in the steep gradient region, even though an enhanced intermittency is observed across all iso-density time traces at the early stage of the ELM. The skewness reveals a predominance of outward excursions of density layers located at the pedestal bottom and of inward movements in the higher density layers: the skewness transits from negative to positive values at a density layer corresponding to a radial position of $\rho_{pol} \approx 0.98$. The observed movements of the density layers are likely related to filamentary activity as it will be shown in the following sections with FFR data obtained with improved time resolution.

3.2. FFR probing

Typical FFR signals, phase $\varphi(t)$ and amplitude $A(t)$, are shown in figure 4 for a period comprising a compound plus a regular type-I ELM, as illustrated in the time trace of the inner divertor shunt currents. The behaviour of both the phase and the amplitude signals during the ELMs (see shaded areas in figure 4) is different from the so called "inter-ELM" periods. Multiple phase jumps occur in the phase signal of both channels throughout the ELM period while a slow drift of the phase is also present in the inter-ELM phase. This is not unusual as phase signals from reflectometry may exhibit a slow continuous drift and/or phase jumps that are often due to one or multiple asymmetries or misalignments in the experimental apparatus/plasma interface resulting in the so-called phase runaway [33].

The signal amplitude also suffers significant modifications during the ELMs: the average amplitude is reduced and the fluctuations are enhanced. The spectra of the various reflectometry signals also show

clear differences between the ELM and inter-ELM periods as depicted in figure 5. The whole spectrum of the complex signal *Aexp(iφ) flattens* out under the influence of the ELM such that the very low frequency components are reduced while the high frequency components are enhanced. This kind of change is also observed in the spectra of the amplitude signals whereas the whole phase spectrum has increased power during the ELM as compared to the inter-ELM period. Both the reduction in the average amplitude of the reflectometry signals and the power spread over the frequency spectra is not surprising taking into acocunt the multiple time- and spatial-scale phenomena associated with the ELM leading to stronger scattering and diffraction effects.

3.3. Novel technique to detect plasma filaments with reflectometry

We can expect that fast coherent density structures propagating in the plasma such as filaments will induce higher radial velocities of the plasma density layers than any background movements induced by broadband turbulence, at least up to some level of density fluctuations (see for instance radial velocity measurements with Langmuir probes in [28]).

In reflectometry, the 1D geometric optical model for wave propagation and reflection, provides a measurement of the radial velocity of the cut-off density layer (V_r) through the time derivative of the reflectometry phase: $V_r = (d(\Delta\varphi)/dt)(c/4\pi F_o)$. Here, we propose to use high absolute values of the phase derivative (from FFR signals) as an indicator of the presence of filaments, of course provided they are within the instrument resolution.

As an example, the ELMy period analysed before in fig. 4 is now shown in fig. 6 where it is displayed the time traces of: two magnetic pick-up coils located on the LFS and poloidally displaced; the $d(\Delta\varphi)/dt$ signal from Q-band channel at 33.0 GHz (probed density $n_{e1} = 1.35 \times 10^{19}$ m^{-3}); the $d(\Delta\varphi)/dt$ signal from V-band channel at 49.4 GHz ($n_{e2} = 3.01 \times 10^{19}$ m^{-3}); the I_{sat} from a Langmuir probe at the maximum depth of the manipulator plunge; and the usual ELM monitor, the inner divertor current.

The ELM signature on the magnetic coils starts almost simultaneously in both signals, suggesting a global character of the ELM *explosive* feature. This takes place some hundred μs before the ELM peaks at the divertor currents.

We observe that reflectometry bursts are well correlated with peaks in the I_{sat}. In particular at the ELM crash where the most active period is observed. The reflectometry bursts observed in the inter-ELM period correspond to I_{sat} peaks of much lower amplitude than those measured by the probe in the ELM period (see for example the time interval just after 2.135s). Reflectometry data displays peaks with similar amplitudes in both ELM and inter-ELM intervals. This probably reflects the differences between the two measuring techniques: the I_{sat} measurement is mainly proportional to the local electron density whereas the phase derivative measurement depends on several local density parameters (amplitude of density fluctuations, velocity and gradient of the local density layer) which results in a complex and more sensitive response.

The time derivative of the reflectometry phase exhibits both positive and negative peaks. This is expected even in the simple picture of the phase derivative being a measurement of the radial velocity as the plasma density layers move back and forward depending on the propagation of density perturbations. To illustrate this simple reasoning consider the “cartoon” in figure 7 where it is shown the reflectometry measurement of a density perturbation propagating with radial velocity and propagating with a poloidal velocity. The trajectory of the filaments across the lines of sight would cause the probed density layer to move outwards and inwards, in both cases. The existence of peaks in the radial velocity of the density layer probed by the reflectometer is also expected. The amplitude and sharpness of those peaks depend on the density profile of the filament and its velocity components, but also of factors like the radial position (in the poloidal propagation case) and of how far the filament travels before its density amplitude drops below the cut-off density (in the radial propagation case).

The poloidal rotation of filaments can thus result in an apparent radial displacement of the density layers. The reflectometry phase signals should display a more complex behaviour as filaments have a fine structure and can propagate with radial, toroidal and poloidal velocity components. In addition, it

is known that the reflectometry phase measurement does not always follow the simple geometric model and can behave in a much more complex way depending on the propagation and reflection conditions of the microwave. Nevertheless, as will be shown in the following sections, either by inducing a fast radial movement of the plasma density layer or by other physical phenomena, filaments will display a clear signature on the time derivative of the phase signals thus providing a sound monitor of plasma filaments.

4. Study of filamentary activity along the ELM cycle

4.1. Filament occurrence

The filament detection method consisted on a peak detection algorithm with a threshold condition applied to the phase derivative signals of the FFR. This technique was applied to study the filament occurrence during the ELM cycle. In fact, we have converted the $d(\Delta\varphi)/dt$ signals of each reflectometer into radial velocity time traces $V_r(t)$ according to the previously given 1D optics relation. By doing so the detection in both instruments was *normalized* to a physically meaningful plasma parameter: the radial velocity of the plasma layers. We selected a threshold of 1.2 km/s in the fluctuating components of the $V_r(t)$ signals based on the following reasoning: (i) it is in agreement with filament detection using data from Langmuir probes; (ii) it is well above the root mean square values of both reflectometry channels (typically 250-500 m/s) and (iii) it is within the range of typical radial velocities of filaments at AUG.

Figure 8 displays results of detection with the Q- and the V-band channels over 20 ELM cycles in the form of probability distribution functions (PDFs). A time scale was defined relatively to each ELM considered (t_0=0 at the peak of each ELM as measured by the inner divertor tile shunt currents - which were pre-conditioned with a 3-point moving average). The individual inner divertor tile currents (synchronized for each ELM) are displayed in black, together with the average ELM signature (in red). The PDFs were built as histograms of the detection times of positive (black) and negative (red) V_r peaks along the ELM cycle for each reflectometer. As a reference, the position of each reflecting layer in the inter-ELM periods was $\rho_{pol} \approx 1.02$ (Q-band) and $\rho_{pol} \approx 0.99$ (V-band).

The distributions of positive and negative peaks are very similar within each channel. The results show that filaments occur during the entire ELM cycle and display maxima occurrence in both channels some 0.5 ms before the ELM produced a peak in the inner divertor tile currents. This observation is in line with filament measurements from Langmuir probes which report that the first filaments start to leave the LCFS some hundred μs before the ELM peaks [28]. The two reflectometer channels reveal that during the ELM the distribution functions are broader in the V-band (probing $n_{ec} = 3.01\text{x}10^{19}$ m^{-3}) extending through the whole ELM phase whereas in the Q-band channel (probing $n_{ec} = 1.35\text{x}10^{19}$ m^{-3}) the increased filament activity goes down to inter-ELM levels shortly after the PDF maximum is achieved. There are several potential interpretations for this result. First, the different poloidal locations of the V- and Q-band antennas might suggest a reduced filamentary activity at the mid-plane compared to below the mid-plane. This effect can most likely be excluded considering the relatively small poloidal angle between the two measurements. Alternatively, the smaller antenna spot-size of the V-band enables detection of smaller filaments compared to the larger Q-band antenna spot-size. This interpretation would be supported by previous filament observations at AUG where the amplitude of filaments indeed decreases towards the end of the ELM [4, 28], as well as by inspection of the I_{sat} behaviour in figure 6. It is plausible therefore that the narrower PDF of Q-band is due to *blindness* of the antenna to filaments with amplitude/size below some critical value.

It can thus be concluded that the abrupt increase of filament activity observed with both reflectometry systems, some hundred μs before the ELM onset, could also be due to filaments of larger amplitude and size scales.

4.2. ELM transport and time-scales

In the PDFs shown in figure 8 all the distributions resemble Gaussian distributions in the vicinity of their maximum. We have fitted those data comprised in the time interval [t_0-2ms, 0] and found that the Q-band maximum consistently precedes the V-band maximum in both positive and negative peak detection cases. The time values corresponding to those maxima are presented in table 1. A time delay analysis can thus be performed if we consider that most of the filaments have propagated in the plasma in such way that they have been measured at the two locations probed by each of the two reflectometers. For example, taking the average values of positive and negative peak cases, we have an *average* maximum at a time of - 461 μs in the Q-band and at - 266 μs in the V-band, leading to a time delay of 195 μs between the measurements at the two locations. The physical displacement between the two measurement spots is approximately 4 cm in the radial direction and 23 cm in the poloidal direction with the V-band measuring spot inwards and downwards relative to the Q-band spot. If we discard any unlikely hypothetical inward movements of the structures, this means that filaments must have propagated downwards with a poloidal velocity component of ≈ 1180 m/s. That is, just before the ELM crash, the majority of filaments at the peak of filament activity propagate with a dominant poloidal velocity component in the ion diamagnetic drift direction (downwards at the LFS with the usual $B_t < 0$).

Table 1. Time coordinate of the maxima found in the detection PDFs (relative to the ELM peak, t_0=0) for both FFR channels and both V_r peak signs.

Channel (band)	Peak (sign)	Time (μs)
Q	+	- 474
Q	-	- 447
V	+	- 278
V	-	- 253

We anticipate that reflectometry is in fact sensitive to the influence of the ELM on transport during the instability growth period since the measurements are performed near the outer mid-plane (region where the ballooning modes are most unstable) and with high temporal resolution. Therefore, the delay between the time of maximum filament activity seen in the outer midplane (Q-band) and the peak of the ELM observed at the inner divertor tile currents ($\tau_{Q\text{-div}}$ = 461 μs) might comprise at least two time scales: the time scale τ^{MHD} over which the MHD processes of the ELM (e.g. non-linear ballooning stage) are flushing particles from the core, and the time scale $\tau_{||}$ over which parallel transport along open field lines outside the LCFS towards the lower divertor is taking place.
The parallel transport time is determined by the less mobile ions ($\tau_{||} \approx \tau^{ions}_{||}$) such that $\tau_{Q\text{-div}} = \tau^{ions}_{||} + \tau^{MHD}$ [34]. A comparison between the experimental time delay and the aforementioned time scales is thus possible.
The time scale $\tau^{ions}_{||}$ is estimated via $L_{||}/c_s$ where $L_{||}$ is the characteristic SOL connection length and c_s is the ion sound speed. Using a field line tracing routine to obtain the parallel connection length from the Q-band measuring spot location to the outer divertor plate ($L_{||}$ = 18m), and assuming the electron and ion temperatures at the separatrix are equal, $T_e = T_i \approx$ 100 eV, we compute $c_s = [(T_e + T_i)/m_D]^{1/2}$ where m_D is the mass of the deuterium ions. In this case we obtain $\tau^{ions}_{||} \approx$ 257 μs. If temperatures at the pedestal top were used instead for the energy ions (≈ 350 eV) the values obtained for $\tau^{ions}_{||}$ would be lower, in the range of 137-186 μs, depending on the $L_{||}$ used (here, $L_{||} = \pi q_{95} R$ would be more suitable).
In addition, τ^{MHD} can be estimated by the time scale of the explosive development of the ballooning filaments throuh $\tau^{MDH} = [(\tau_A)^2\ \tau_E]^{1/3}$ where τ_A is the shear Alfvén time and τ_E is the global energy confinement time [35]. In this plasma discharge we estimate the Alfvén velocity $V_A \approx 7.3 \times 10^6$ m/s and therefore $\tau_A = a/V_A$, where a is a characteristic length ($a=\pi q_{95} R$). Together with the energy confinement time $\tau_E \approx 0.2$ s we obtain τ^{MDH} = 130 μs. The whole ELM lifetime prediction can then be

presented as $(\tau^{MDH\_theory} + \tau^{ions}_{\parallel}) = (130+257) = 387$ μs which is in good agreement with $\tau_{Q\text{-}div} = 461$ μs, given the approximations used. This agreement between experimental and expected time scales, and also with previous infrared thermography measurements [36], further confirms both the MHD trigger mechanism of the ELM as being of explosive ballooning nature and the dominant loss channel for ELM filaments, as being the ion parallel transport.

4.3. Filament characteristics from conditional averaging of FFR signals

Having previously established a detection technique we are able to study the signatures of filaments in FFR signals by employing a conditional averaging (CA) technique [37]. This method allows extracting the coherent fraction of a signal if a large ensemble of data consisting of time windows centered on the detection times can be gathered. The conditional averaging can also be performed on any suitably synchronized signal, other than the one used for event-detection, in order to look for possibly correlated signatures, e.g. between the two Q and V reflectometry channels. The radial velocity $V_r(t)_{ch1}$ signal from one of the reflectometry channels is used to detect filaments while we use as *secondary* signals: the phase $\varphi(t)_{ch1}$ and amplitude $A(t)_{ch1}$ from the channel used for detection, and the three corresponding signals from the other reflectometry channel, $V_r(t)_{ch2}$, $\varphi(t)_{ch2}$ and $A(t)_{ch2}$. Using again as time reference (t_0=0) the ELM peak in the inner divertor tile currents and taking into account the average ELM length, we define three periods: the ELM onset period [t_0-1ms, t_0]; the ELM period [t_0, t_0+2ms]; and the inter-ELM period, outside the time periods [t_0-2ms, t_0+6ms].

Typical results from the CA method obtained with the Q-band system (only positive peak detection) are shown in figure 9, The very narrow peaks, and the somewhat broader dips observed respectively in V_{r_ch1} and A_{ch1} signatures from CA, are typical features of the results obtained with this technique when using both the Q-band and the V-band (not shown here) channels. It is found that most of the results obtained with the detection of negative peaks display a similar picture as the corresponding positive peak case but with an inverted phase jump. The amplitude dips suggest the occurrence of either negative interference or diffraction effects. The latter is reasonable when considering the oblate density profile of the filaments. Note that similar trends are found when using any of the channels. The main differences in the signatures of the filaments over the different periods are in the absolute values of the peaks and dips in each period. The greatest impacts on V_{r_ch1} and A_{ch1} signatures are found in different periods: the largest V_r peak values are in the ELM onset period (where the smallest A_{ch1} dip values are found), while the largest A_{ch1} dip values are in inter-ELM periods (together with the smallest V_r peak value). While the larger V_r peak values found during the ELM onset period may be due to effectively higher radial velocity components of the propagating structures, the maximum amplitude dips in the inter-ELM periods might be explained by a better background reflection, leading to a relatively higher signal loss due to the filament measurement, comparing to the ELM periods.

The detection "frequency" of filaments along the ELM cycle is shown in the top trace of figure 10 for both reflectometry bands, and for positive and negative events. The figure shows the total number of events detected (peaks found with a threshold of 1.2 km/s) divided by the total time length of all intervals considered. Positive and negative events (V_r peaks of opposite direction) were found with very similar frequencies. We can also observe that in the ELM periods the detection frequencies are higher in the (inner) V-band than in the Q-band, but during inter-ELMs the situation is reversed. This could mean that either a large fraction of inter-ELM filaments are generated further outwards than during ELMs, or closer to the mid-plane. Still, comparing the Q-band and the V-band results we observe that the V_r peak values are always higher in the Q-band, regardless of the period considered. This could mean that filaments are being detected in a region where they always accelerate outwards or decelerate downwards. It is important to note that a comparison of absolute amplitude values between both channels is not meaningful as the systems have different antennas and amplifier gains.

4.4. Filaments and MHD in inter-ELM periods

The signatures obtained with positive peak detection (figure 9), showed that the phase signatures consist of phase jumps of increasing height and duration, when going from the inter-ELM period to

the ELM onset period, with intermediate scales at the in-ELM periods. This is in line with the previous hypothesis that at the ELM onset filaments would be larger. Despite this fact, the inter-ELM periods are in principle a more favourable scenario for additional analysis of filament signatures since the background reflection is stronger as the density profile is not perturbed as in the ELM periods. The signatures obtained in the inter-ELM periods are shown in figure 11, where we have used a larger CA time window of 1900 μs and both Q-band and V-band signals for detection. Here we have also considered the fluctuating components of the phase signals ($\varphi(t) - \langle\varphi(t)\rangle$) instead of the original full-phase signals to remove any long-term background trends. The signatures obtained with the Q-band detection display a strikingly symmetric picture between the positive and the negative peak detection cases. In the light of 1D geometric optics, this symmetry could be explained by a combination of opposite density perturbations (a *blob* and a *hole* in the density profile) and/or the direction of their radial propagation. The sign of the phase response together with the symmetry axis (time or phase) could help to pin down the probable cause from the above possibilities but the shape of the signatures makes this task totally ambiguous. Note that a large filament propagating in the poloidal or toroidal direction across the line of sight would appear as a density blob when entering the measuring spot and as a density hole when leaving the probed region. However, 2D models suggest that in some cases (e.g. of a high enough amplitude of the density perturbation together with a misaligned antenna) the phase response can flip direction (opposite to the displacement of the density layer) at some critical value of the perturbation amplitude [33].

The signatures obtained with the V-band detection also exhibit some symmetry between the positive and the negative peak detection cases. In addition, a fairly well correlated measurement in the phase signals of the Q-band is present. The case where the V-band channel is used for detection of positive peaks is displayed in the right plot of figure 11 together with the *secondary* signal obtained with the Q-band and the cross-correlation function between both signatures.

Assuming again that the individual coherent structures were measured by both reflectometers then the cross-correlation maximum shows that the filaments propagated from the Q-band to the V-band measurement spot, i.e. either downwards poloidally or inwards radially. Applying the same reasoning we arrive to a dominant poloidal velocity in the ion diamagnetic drift direction (consistent to what we obtained for the ELM onset period) with a value of $V_\theta \approx 575$ m/s.

If we now take the width of the phase signatures around the detection time (ranging in [100-200] μs) as the filament observation time t_{obs}, we are able to estimate an average poloidal size of the detected filaments. Using $S_\theta = V_\theta\, t_{obs}$ we obtain the range $S_\theta \approx$ [5.75 - 11.50] cm which agrees with the literature and is within a "measurable" size for both reflectometry systems. Taking the typical field line inclination ($\alpha = 10^o$) we can also expect that filaments should have a minimum toroidal size S_ϕ estimated by $S_\phi = S_\theta / \sin(\alpha)$ which ranges in $S_\phi \approx$ [33-66] cm.

Wave-like signatures

Both the phase signatures and the cross-correlation of the positive-peak detections with V-band display a wave-like signature of few cycles of oscillation with a frequency of the order of ≈ 1.7-2.5 kHz. This frequency is much lower than ELM MHD precursor frequencies typically observed at AUG, of some tens of kHz which could be occurring around these time periods [38]. This wave-like signature could nevertheless arise from the development of the peeling-ballooning mode and be an effect of the toroidicity of the filaments themselves. Taking into consideration this oscillatory nature (with a *period* $T' \approx$ [400-600] μs), we can also give an estimation of the poloidal separation between adjacent filaments as $\Delta_\theta = V_\theta\, T'$ and therefore a characteristic poloidal mode number (m), as $m = 2\pi r / \Delta_\theta$, where r =0.44 m is the minor radius. We obtain the following ranges: $\Delta_\theta \approx$ [23.0-34.5] cm and therefore $m \approx$ [8-12]. From the known relation $q = m/n$, and taking q_{95}, also the toroidal mode number (n) can be computed, which falls in the range $n \approx$ [2-3]. These toroidal mode numbers are less than those usually computed for ELM filaments but they are consistent with the picture that at the explosive period they have evolved from lower mode numbers [36].

5. Discussion and conclusions

A novel technique for detection of plasma filaments was developed based on the time derivative of the phase signals obtained with fixed frequency reflectometry (FFR). We have demonstrated that the peaks in those signals (high absolute values) provide a sound indicator of the presence of filaments, as detection results compared favourably with Langmuir probe data. The novel method was applied to study filamentary activity during the ELM cycle, in a region close to the separatrix, together with a conditional averaging technique.

Under the 1D geometric optics approximation the time derivative of the FFR phase is a measurement of the radial velocity of the probed density layer and therefore we expected filaments to produce both positive and negative peaks in this FFR signal. The results confirm this reasoning as detection of both peak signs produced equivalent detection frequencies and PDFs.

The occurrence of filaments throughout the ELM cycle was observed to be ubiquitous yet displaying a clear maximum some hundred microseconds before the peak of the ELM (currents) at the divertor. The propagation of filaments in that period (ELM onset) was found to display a dominant poloidal velocity component in the ion diamagnetic drift direction. The same conclusion could be drawn for the inter-ELM filaments despite being based on a different time-delay technique. In this case the CA signatures in both FFR channels were correlated. Further support to the observation that the majority of detected filaments travel with dominant poloidal velocity component lies in the filament signatures obtained with CA: phase jumps and amplitude dips as, expected from numerical simulations in the cases of poloidally propagating perturbations, namely a Gaussian perturbation plus a misaglined reflection case, or a sawtooth-like perturbation in aligned geometry [33]. The fact that the signatures in both FFR channels were not correlated in the ELM periods might be a result of broader filament velocity distributions, or merely of an increased radial velocity component of the ELM filaments making it impossible for a filament to travel the large poloidal distance between the two measuring spots. Both of the above explanations are plausible. Nevertheless, the values and direction of the filament poloidal velocity component agree with previous measurements at AUG [28].

The above results indicate that the (majority) peaks used for filament detection in the V_r signals are due to radial displacements of the cut-off density layer as a result of poloidal propagation of filaments, and not due to an effective radial propagation of filaments.

The mechanisms proposed in literature to explain the ELM development and energy losses were in part confirmed by the reflectometry measurements: a wave-like signature appeared together with the filament detection and it was possible to estimate poloidal and toroidal mode numbers that agree with the expected MHD instability in the linear growth regime. Furthermore, the expected time scales involved in the ELM explosive period and those measured by FFR and the divertor currents were also in good agreement.

In order to further validate the experimental findings and to obtain further information from the reflectometry measurements, a 2D full wave code (see [39]) is being applied to emulate the filament measurements performed with reflectometry. Also, the hopping possibilities of the reflectometry diagnostic will be explored to investigate a broader probing area, from the separatrix up to the pedestal top. The possibility to distinguish filaments with different dominant velocity components (radial or poloidal) *via* refinement of the method or detection criterion is also left open for future investigations.

Acknowledgments

This work was supported by EURATOM and carried out within the framework of the European Fusion Development Agreement. IST activities also received financial support from "Fundação para a Ciência e Tecnologia" through project Pest-OE/SADG/LA0010/2013. The views and opinions expressed herein do not necessarily reflect those of the European Commission.

References

[1] A. Kirk *et al* Phys. Rev. Lett. **92** (2004) 245002

[2] A. Kirk *et al* Plasma Phys. Control. Fusion **47** (2005) 995-1013

[3] B.D. Dudson *et al* Plasma Phys. Control. Fusion **50** (2008) 124012
[4] A. Kirk *et al* Plasma Phys. Control. Fusion **53** (2011) 095008
[5] P.B. Snyder *et al* Plasma Phys. Control. Fusion **46** (2004) A131
[6] H.R. Wilson and S.C. Cowley, Phys. Rev. Lett. **92** (2004) 175006
[7] H.W. Müller *et al* Nucl. Fusion **51** (2011) 073023
[8] B. Nold *et al* Plasma Phys. Control. Fusion **52** (2010) 065005
[9] S.I. Krasheninnikov Phys. Lett. A 283 (2001) 368-70
[10] O.E. Garcia *et al* Phys. Plasmas **13** (2006) 082309
[11] W. Fundamenski *et al* Plasma Phys. Control. Fusion **48** (2006) 109-156
[12] C. Silva *et al* J. Nucl. Mater. 390-391 (2009) 355-358
[13] H. Tanaka *et al* Nucl. Fusion **49** (2009) 065017
[14] G.S. Kirnev *et al* Nucl. Fusion **45** (2005) 459-467
[15] E. Mazzucato, Rev. Sci. Instrum. **69**, No.6 1201 (1998)
[16] G.D. Conway, Nucl. Fusion **46** (2006) S665
[17] V.V. Bulanin *et al* Techn. Phys. Lett. **37** (2011) 340-343
[18] H. Zohm *et al* Nucl. Fusion **49** (2009) 104009
[19] L. Cupido *et al* Rev. Sci. Instrum. **77** (2006) 10E915
[20] Chien-ming Wu *et al* Meas. Sci. Technol. **7** (1996) 520-524
[21] G. Wang *et al* Nucl. Fusion **46** (2006) S708
[22] N. Bretz Phys. Fluids B **4** (1992) 2414
[23] A. Silva, Final Project of Bachelor degree, Instituto Superior Técnico (1988)
[24] G.D. Conway, Plasma Phys. Control. Fusion **39** (1997) 1261
[25] A. Silva *et al* Rev. Sci. Instrum. **72** (2001) 320
[26] M.E. Manso *et al* Plasma Phys. Control. Fusion **43** (2001) A73-A93
[27] S. Hacquin *et al* Proc. 28th EPS Conf. on Contr. Fusion and Plasma Phys. Funchal, 18-22 June 2001, ECA Vol.**25A** (2001) 1209-1212
[28] A. Kirk *et al* Plasma Phys. Control. Fusion **53** (2011) 035003
[29] M. Kočan *et al* Nucl. Fusion **53** (2013) 073047
[30] D. Carralero *et al* Europhysics Conference Abstracts **37D** (2013) O4.108
[31] G. Fuchert *et al* 'Blob properties in L- and H-mode from gas-puff imaging in ASDEX Upgrade' (to be published in)
[32] J.E. Boom *et al* Nucl. Fusion **51** (2011) 103039
[33] G.D. Conway, Plasma Phys. Control. Fusion **41** (1999) 65-92
[34] T. Eich *et al* J. Nucl. Mater. 337-339 (2005)
[35] S. Cowley *et al* Plasma Phys. Control. Fusion **45** (2003) A31
[36] T. Eich *et al* Plasma Phys. Control. Fusion **47** (2005) 815-842
[37] D. Block *et al* Phys. Scr. **T122** (2006) 25-33
[38] T. Kass *et al* Nucl. Fusion **38** (1998) 111-116
[39] F. da Silva *et al* Rev. Sci. Instrum. **72** (2001) 311

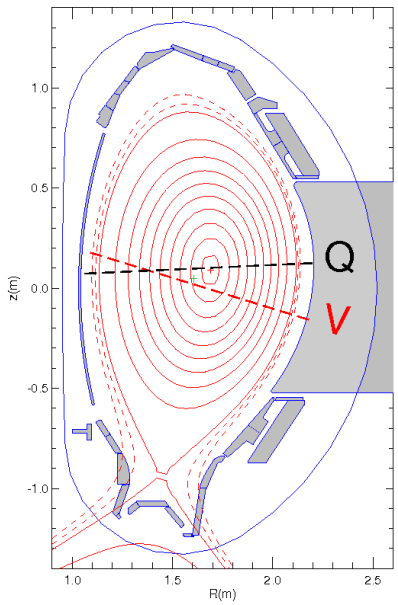

Figure 1. Poloidal cross-section of the AUG vessel. Poloidal flux surfaces in LSN configuration (#26981, t=2.1s) and lines of sight of the Q- and V-band FFR systems are shown.

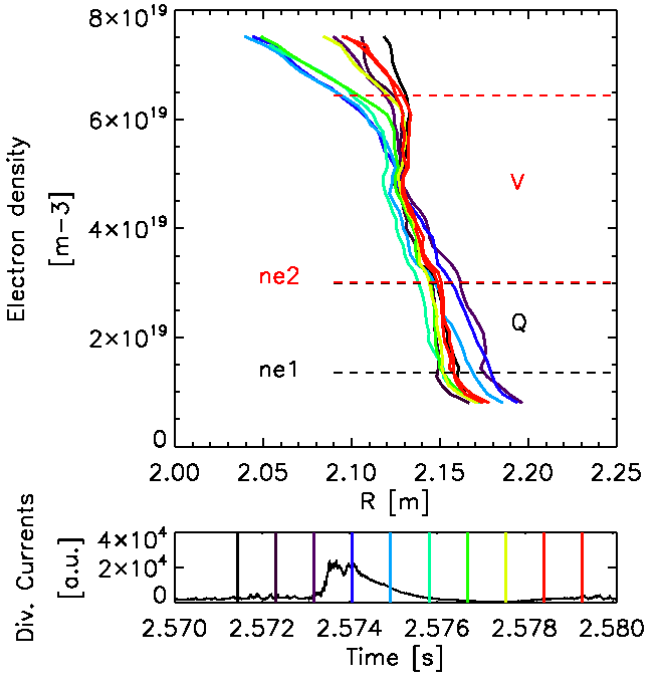

Figure 2. Edge density profiles from FM-CW reflectometry in the vicinity of an ELM (AUG discharge #25557: LSN, Ip = 1.15 MA, B_t = -2.5T, q_{95} = 4.1, P_{ECRH} = 0.5 MW, P_{NBI} = 5.0 MW, $\overline{n_e}$ = 8.1 x10^{19}m^{-3}). The density ranges that can be probed by both the Q-band (1.35 – 3.00) x10^{19}m^{-3} and the V-band (3.01 – 6.43) x10^{19}m^{-3} channels are shown within dashed lines. The time trace of the inner divertor current is shown below with time stamps coloured as the corresponding density profile.

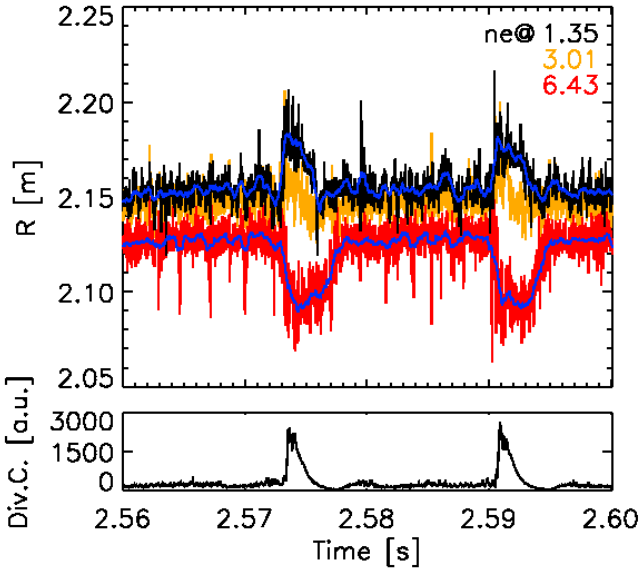

Figure 3. Evolution of the radial position of selected density layers (1.35, 3.01 and 6.43 x10^{19}m^{-3}) along a type-I ELMy H-mode period (#25557, R_{sep} = 2.148 ± 0.005 m). Data was obtained from FM-CW profiles with 35us time resolution. Moving averages with 16 data points (profiles) are also depicted in blue lines.

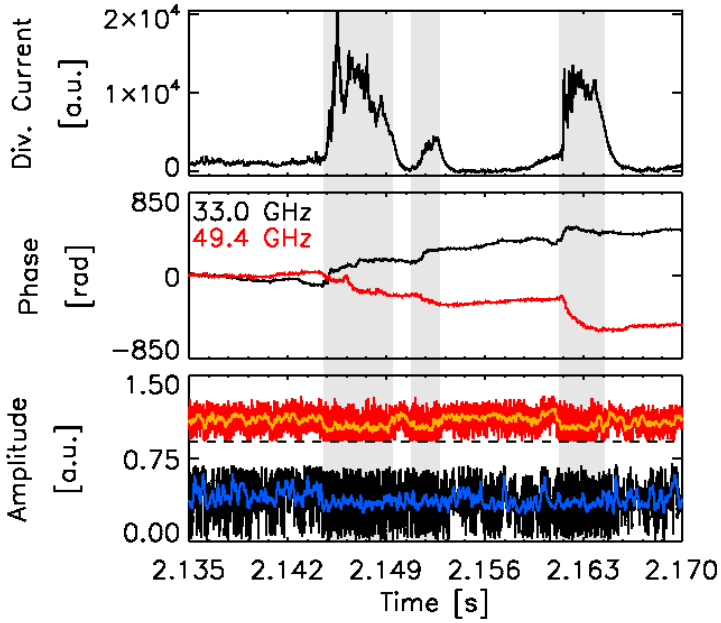

Figure 4. FFR signals (phase and amplitude) from Q-band and V-band systems operating at their lowest frequencies - 33 GHz and 49.4 GHz (density layers 1.35 x10^{19}m^{-3} and 3.01 x10^{19}m^{-3}) along a type-I ELMy H-mode (#26981). An offset was introduced in the V-band amplitude signal for better visualization. The inner divertor current is shown on the top plot.

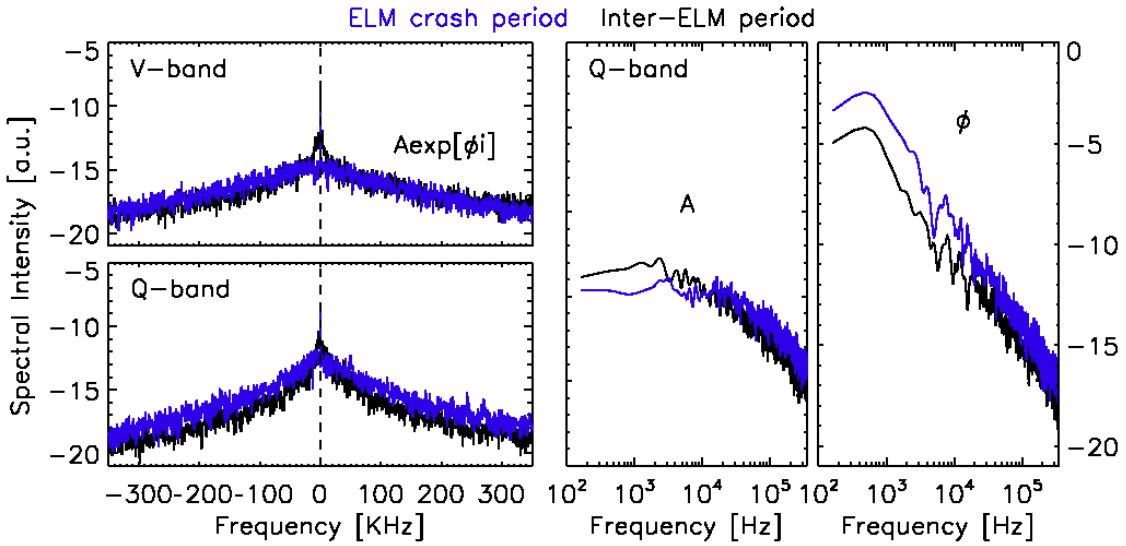

Figure 5. Comparison between inter-ELM and ELM periods: Fourier spectra of FFR signals from both hopping systems at their minimum operational frequency. Spectra of the FFR (complex) output signals displayed in the left. Spectra of the amplitude and phase signals displayed in the right (Q-band channel only).

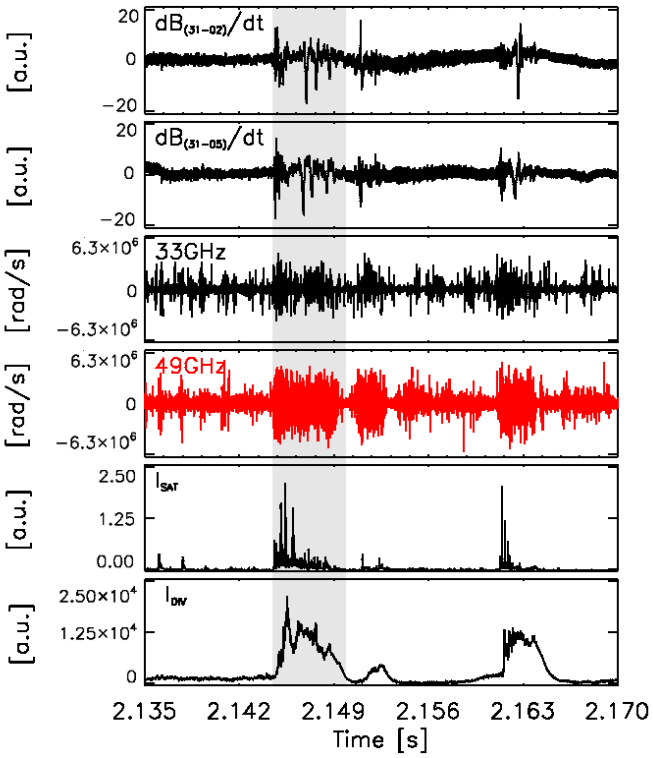

Figure 6. Time traces from several diagnostics during a type-I ELMy H-mode. From top to bottom: two magnetic coils poloidally displaced (B31-02 at the mid-plane and B31-05 below the mid-plane), dφ/dt signals from both hopping reflectometers operating at their lowest frequencies, ion saturation current measured with a Langmuir probe mounted on the manipulator (at the maximum depth of the plunge), and the inner divertor current.

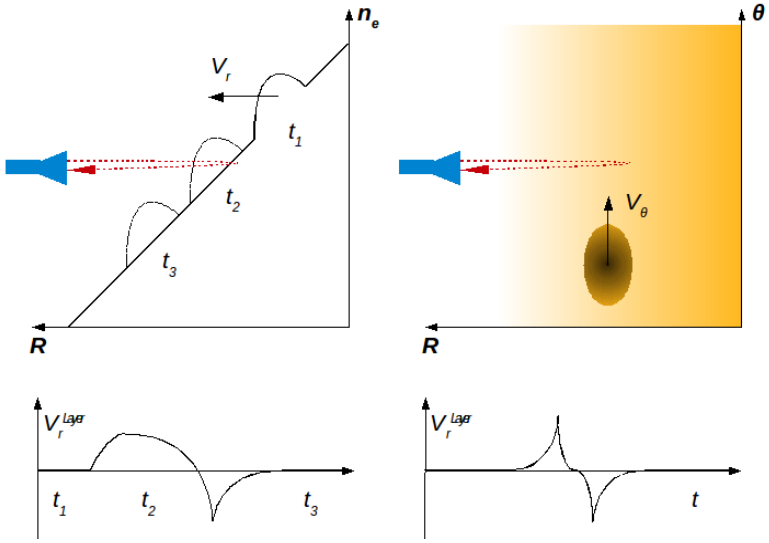

Figure 7. Artist view of the FFR measurements of a plasma filament superposed on a linear background density profile propagating in the radial direction (left) and propagating in the poloidal direction (right) with constant velocity. The hypothetical behaviour of the radial velocity in the density layer being probed is presented for both cases.

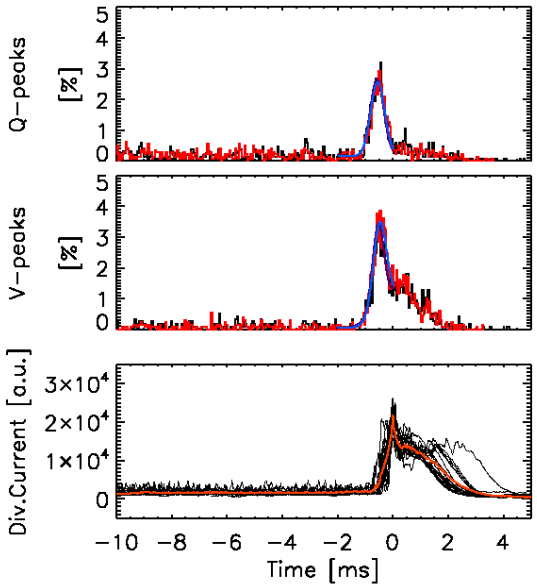

Figure 8. PDFs of the times of detection of positive (black) and negative peaks (red) in the FFR d(φ)/dt signals along the type-I ELMy H-mode cycle. Detection was performed using both channels (Q-band on top and V-band in the middle plot) and histograms built with bins of 50 μs. Fitted profiles to Gaussian distributions are shown in blue lines. The inner divertor current around each ELM comprised in the analysis (black) and their CA (orange) are shown in the bottom plot.

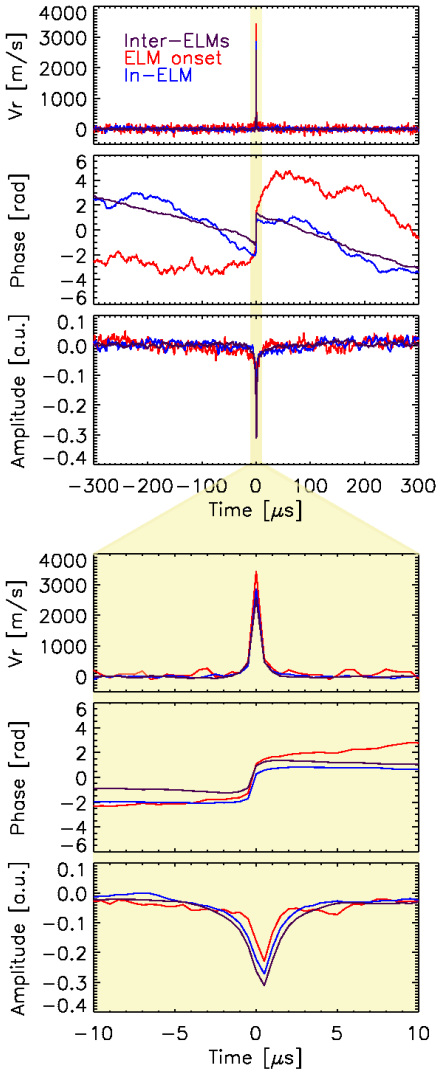

Figure 9. Filament signatures on reflectometry signals obtained with a conditional averaging technique. Events were detected using $V_r(t)$ from Q-band as primary signal (detection threshold at 1.2 km/s and time window of 600 μs) and A(t), φ(t) as secondary signals. A zoom on the results is also shown using a time interval of 20 μs around the detection time.

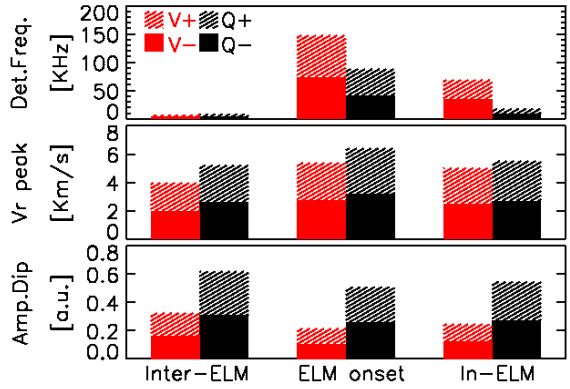

Figure 10. Characteristics of V_r peak detection and CA signatures in different periods of the ELM cycle for both Q-band and V-band channels. Results were obtained from CA with a detection threshold of 1.2 km/s and time window of 600 μs.

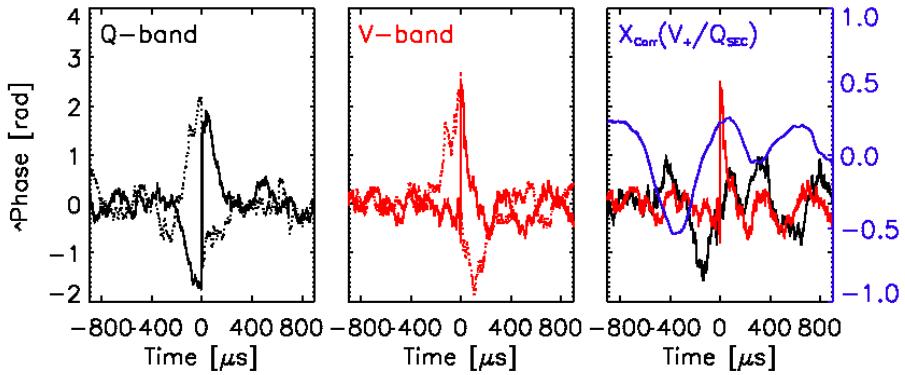

Figure 11. Signatures of inter-ELM filaments on the fluctuating component of the phase signals (detection threshold at 1.2 km/s and time window of 1800μs). The results from positive (solid lines) and negative peak (dotted lines) detections are shown for each band (Q-band in the left and V-band in the middle). Signatures from positive peak detection with the V-band and from Q-band used as secondary in the CA technique are shown in the right plot. The cross-correlation between those signatures is also shown in blue.